

Superconductivity in twisted bismuth bilayers

Isaías Rodríguez¹, Renela M. Valladares², David Hinojosa-Romero¹, Alexander Valladares², Ariel A. Valladares^{1*}.

¹Instituto de Investigaciones en Materiales, Universidad Nacional Autónoma de México, Apartado Postal 70-360, Ciudad Universitaria, CDMX, 04510, México.

²Facultad de Ciencias, Universidad Nacional Autónoma de México, Apartado Postal 70-542, Ciudad Universitaria, CDMX, 04510, México.

*Corresponding Author: Ariel A. Valladares, valladar@unam.mx

Abstract

First-principles calculations for two twisted bismuth bilayers, each with 120 atoms, were studied by means of the electronic density of states and vibrational density of states. Metallic character at the Fermi level was found for the non-rotated sample as well as for each sample rotated 0.5°, 1.0°, 1.5°, 2.0°, 2.5°, 3.0°, 4.0°, 5.0°, 6.0°, 7.0°, 8.0° and 10° with respect to the static bilayer. Assuming that the superconductivity is BCS-type and the invariance of the Cooper pairing potential, we predict a maximum superconducting temperature $T_c \sim 1.8$ K for a magic angle of 0.5° degrees between the two bilayers, increasing the superconducting transition temperature from the experimentally measured value of 0.53 mK for the Wyckoff structure of crystalline bismuth.

1

Introduction

For more than 100 years superconductivity has been present in scientific research. Sometimes in the forefront, sometimes in the background, but the hope of finding high temperature superconductors, the holy grail of technology, has prevail over a century. This discovery would certainly revolutionize several fields of knowledge and technology. Up to the present, disappointment has been the result of multiple claims of having found superconductivity at room temperature. Investigations of materials at high pressures have given hope, once more, towards this discovery, however some of these claims are either for very high pressures [1–4], or for new materials that have not been reproduced worldwide [5–8]. High pressure experiments are very difficult to conduct since the pressures needed, of the order of giga pascals, can only be applied for very short times. One should ask whether pressures below atmospheric may be a different and promising way to approach the problem [9–12]. On the other hand, the new materials so far reported have to be validated by several laboratories to accomplish credibility. Some known materials, like the Xenos [13,14], have also been the subject of study in this quest.

Xenos are a class of two-dimensional (2D) single-element layered materials, primarily derived from group IV elements like carbon (graphene) [15], group V elements like phosphorus (phosphorene) [16], or group VI elements like tellurium (tellurene) [17]. These materials demonstrated unique physical and chemical characteristics against the corresponding three-dimensional (3D) structures.

Xenos have sparked interest due to their tunable properties and potential applications in electronics and photonics [18]. Xenos electronic and lattice dynamics properties can be

engineered by various techniques, like adjusting the lattice structure, doping the layers, twisting the layers, etc.

Bismuth xenes, also known as bismuthenes, have several 2D layered allotropes that have been predicted theoretically [19,20], and at least two of these phases have been experimentally confirmed [21,22]. The first one is an α - phase also known as Bi(110) and consist of puckered orthorhombic structures similar to black phosphorous, while the β - phase also known as Bi(111) consists of a buckled honeycomb-like structure similar to silicene [20,21,23].

Bismuthene, as several other xenes, have been the subject of much interest and investigation as a topological insulator (TI) [24–27]. However, the discovery of superconductivity in twisted bilayer graphene (TBG) [28,29] opens up a new field of study for bismuthene.

Bismuth superconductivity was discovered in amorphous bismuth (*a*-Bi) [30–32] with a critical transition temperature, T_c , of ~ 6 K, while superconductivity in crystalline bismuth (*x*-Bi) was for the first time predicted to have a T_c lower than 1.5 mK [33], and later measured with a T_c of 0.53 mK [34]. While the other stable crystalline phases of bismuth at high pressure were studied finding a maximum of $T_c \sim 8$ K for the Bi-V phase [35,36]. In bismuth bilayers a possible T_c of ~ 2.6 K was found [37].

Here we report the possible superconductivity in twisted bismuth bilayers (TBB) of two bilayers of about 5.1 nm long and 4.2 nm wide, that were twisted with respect to one another at angles of 0.5° , 1° , 1.5° , 2° , 2.5° , 3° , 4° , 5° , 6° , 7° , 8° , 9° and 10° forming different Moiré patterns.

Method

A supercell was constructed starting from the Bi-I (Wyckoff) structure and multiplying it by $10 \times 8 \times 2$ obtaining a 960-atom structure, (see Figure 1 A). Then atoms were removed to end with two 120 atoms bilayers for a total of 240-atoms, (Figure 1 B). To avoid possible self-interactions, and to maintain the structure of two infinite bilayers with the original interatomic structure, the periodic boundary conditions were removed, and we ended with the initial structure of two 120 atoms bilayers, (Figure 1 C). Finally, one of the two nanolayers from the initial structure was rotated around the perpendicular Z axis 0.5 , 1.0 , 1.5 , 2.0 , 2.5 , 3.0 , 4.0 , 5.0 , 6.0 , 7.0 , 8.0 , 9.0 , and 10.0 degrees, obtaining 13 different structures, each with a different Moiré pattern, (Figure 1 D).

Then, electronic density of states ($N(E)$) and vibrational density of states ($F(\omega)$) were calculated using DMol³, a first principles simulation code included in the Dassault Systèmes Materials Studio Suite [38,39]. To obtain the $N(E)$, a single-point energy calculation was performed using a double numerical plus polarization functions basis set (dnp), the density functional semi-core pseudo-potential (dspp) was used for the core treatment, the Vosko-Wilk-Nursair exchange-correlation functional was considered within the local density approximation (LDA) [40], a fine integration grid with octupolar angular momentum fitting functions was incorporated. The real-space cutoff radius for the orbitals was set to 6.0 Å.

The $F(\omega)$ was calculated with the finite displacement method (frozen-phonon method), using the same electronic parameters as the $N(E)$ calculation, and a finite difference of 0.005 Å to obtain the Hessian matrix.

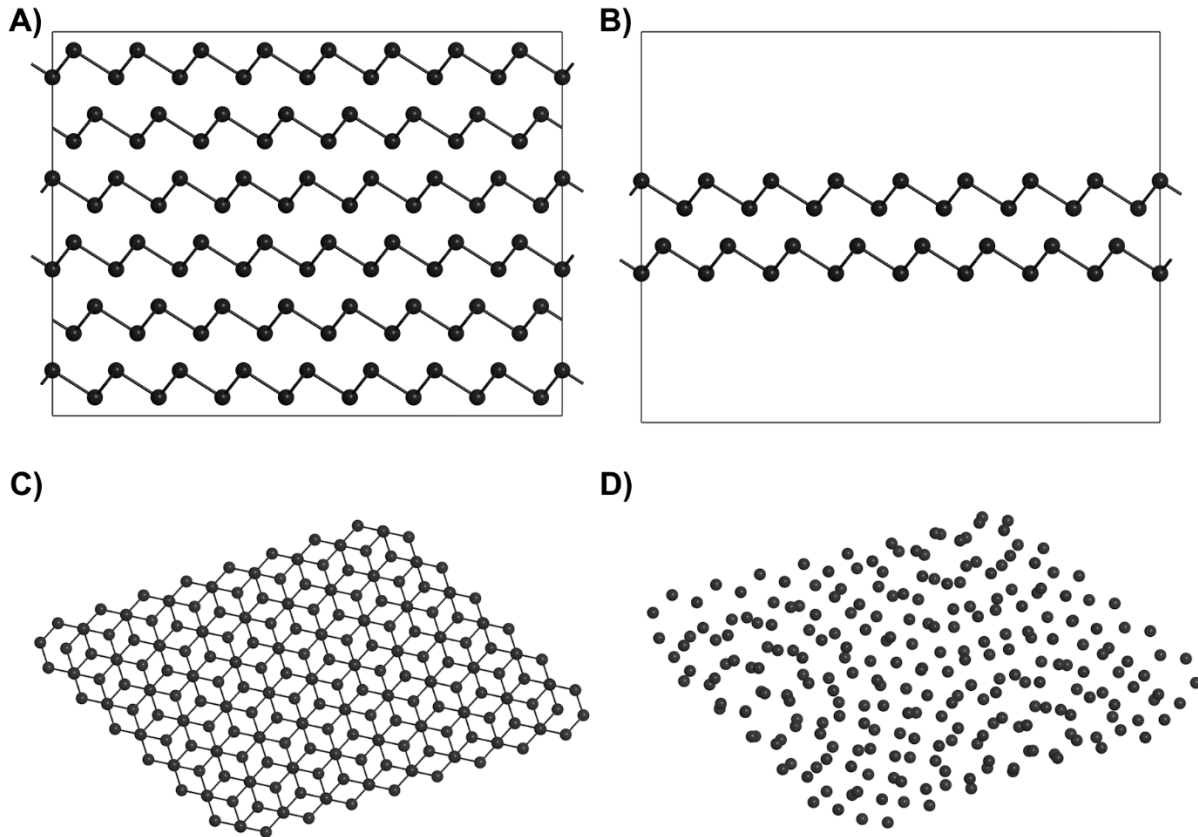


Figure 1. Construction of the Bismuth bilayers. A) 10x8x2 supercell of Bi-I (Wyckoff). B) Isolation of two bilayers of 240 atoms. C) Superior view of the two bilayers without periodic boundary conditions. D) 10° rotation of one of the layers with respect to the other; bond-sticks were omitted in D) in order to better appreciate the Moiré pattern.

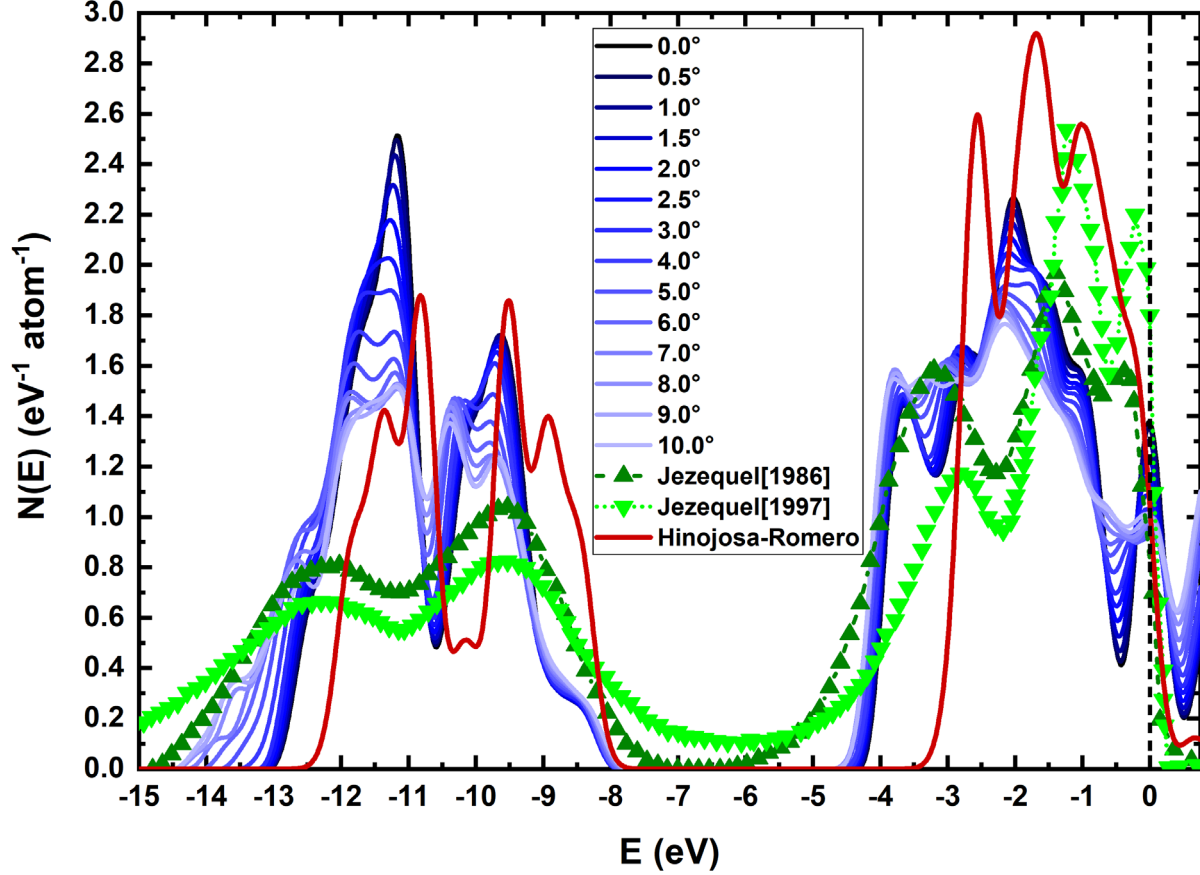
Then the Debye frequencies and Debye temperatures were calculated using the obtained $F(\omega)$ and the method proposed by Grimvall [41]:

$$\omega_D = \exp\left(\frac{1}{3} + \frac{\int_0^{\omega_{max}} \ln(\omega)F(\omega)d\omega}{\int_0^{\omega_{max}} F(\omega)d\omega}\right),$$

$$\theta_D = \frac{\hbar\omega_D}{k_B}.$$

Electronic Density of States

For the $N(E)$ determination, the DMol³ analysis tool included in the Materials Studio suite was used, set to eV and an integration method with smearing width of 0.1 eV. The number of points per eV was set to 100. The results were smoothed and analyzed by means of the OriginPro software using a Fast Fourier Transform (FFT) filter of 3-step [42]. The results are given in states per eV per atom in Figure 2.



4

Figure 2. Comparison of the electronic density of states ($N(E)$) for twisted bismuth bilayers (TBB). Fermi Level is shown as the dashed vertical line. The electronic density of states is normalized per atom. Experimental results from Jezequel (1986) [43] and Jezequel (1997) [44] in green triangles. DFT calculations from Hinojosa-Romero in red [37].

The $N(E)$ is composed of two main bands; the first is bimodal and goes from around -14 eV to -8 eV, this first band includes the majority of s-electron contributions, while the second band is located from around -4.7 eV to above the Fermi level, this second band has contributions from the p-band and d-band electrons, with a small proportion of s-band electrons. For all studied samples, the density of states at the Fermi level ($N(E_F)$) is in a non-zero valley, which is characteristic of the semimetals, as is the case for most of the phases of bismuth [36]. Both of these bands have a small decrease in its height while increasing its width. This is common in structures under external stress as is the case for compressed bismuth [12]. This may indicate the presence of internal forces in the studied samples, such as the mechanical deformation required for the fabrication of the TBG [28,29].

The studied samples have a Van Hove Singularity (VHS) in the $N(E)$ at the Fermi level (Figure 2), these sudden increases in the $N(E)$ are also present in TBG [45–47] as well as in Moiré nanolayers [26], and it seems to be caused by an almost flat band near the Γ point. However, the presence of VHS near the Fermi level has not been detected, neither in the Bi crystalline structure [33,36] nor in the Bismuth (111) bilayers [26,37,48–50]. The VHS seems to be caused by the local density of states of the border atoms.

To correctly represent the electronic density of states of a larger bismuthene bilayer [26,37,48–50], as well as the crystalline results [33,36], it was decided to study the partial electronic density of states of the backbone (center) of the bilayer disregarding the first 4 atoms from the border on each side of the nanosheets; the partial electronic density of states can be seen in Figure 3. The partial eDoS for the backbone is also represented by two bands, but the VHS near the Fermi level is substantially decreased and completely disappears for several of the studied samples (Figure 3), which corresponds to all the studies in the literature for bismuth and bismuthene. This seems to indicate that the VHS present in the total eDoS is mostly caused by border defects. A more detailed study is currently undergoing and will be reported elsewhere.

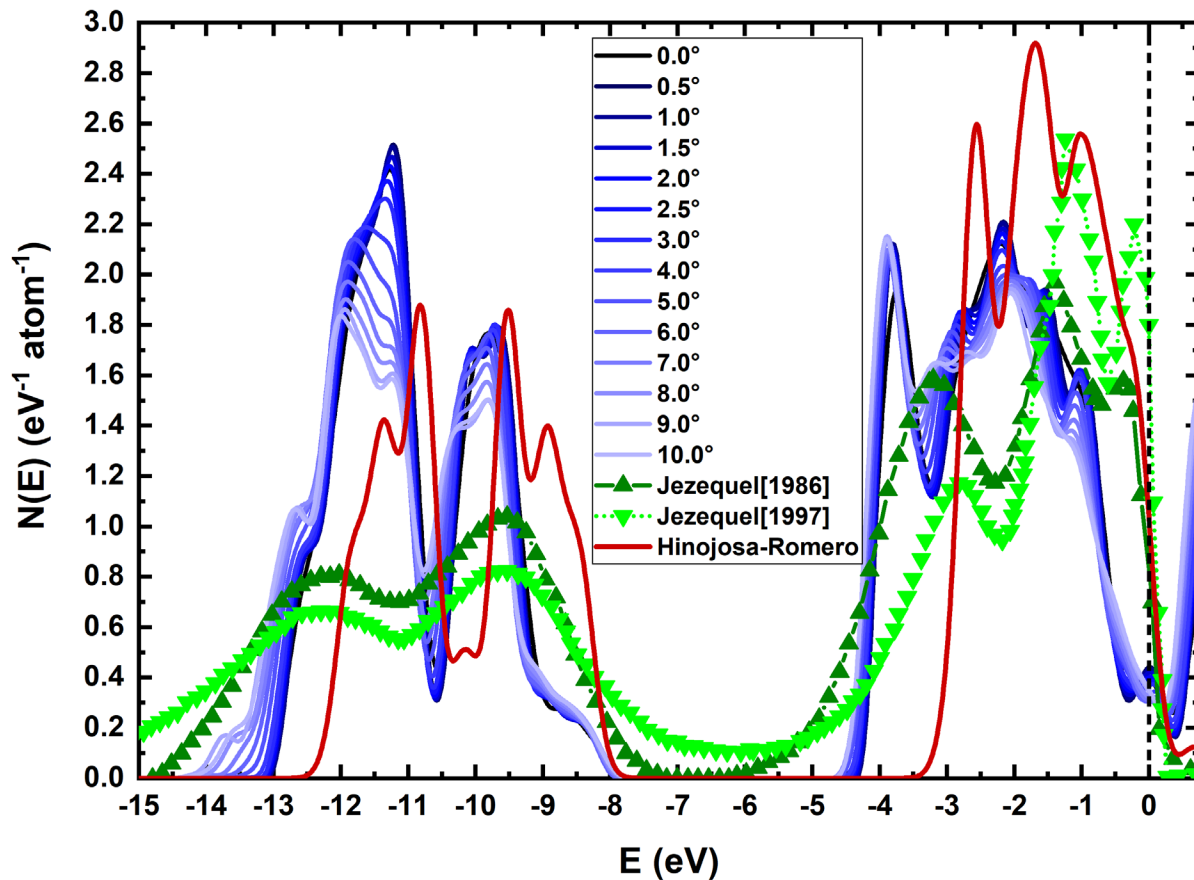


Figure 3. Comparison of the partial electronic density of states ($N(E)$) for the backbone (center) of twisted bismuth bilayers (TBB). Fermi Level in vertical dashed line. The electronic density of states is normalized per atom in the nanolayers. Experimental results from Jezequel (1986) [43] and Jezequel (1997) [44] in green triangles. DFT calculations from Hinojosa-Romero in red [37].

Vibrational Density of States

For the $F(\omega)$ the results were analyzed with OriginPro software [42], using the normal modes calculated in meV with DMol³. To obtain the $F(\omega)$ a frequency count with a 0.1 meV bin width was used, then the resulting histograms were smoothed with a three-step FFT filter. The translational modes around 0 were removed. Finally, the $F(\omega)$ s were normalized to 3, these results can be seen in Figure 4.

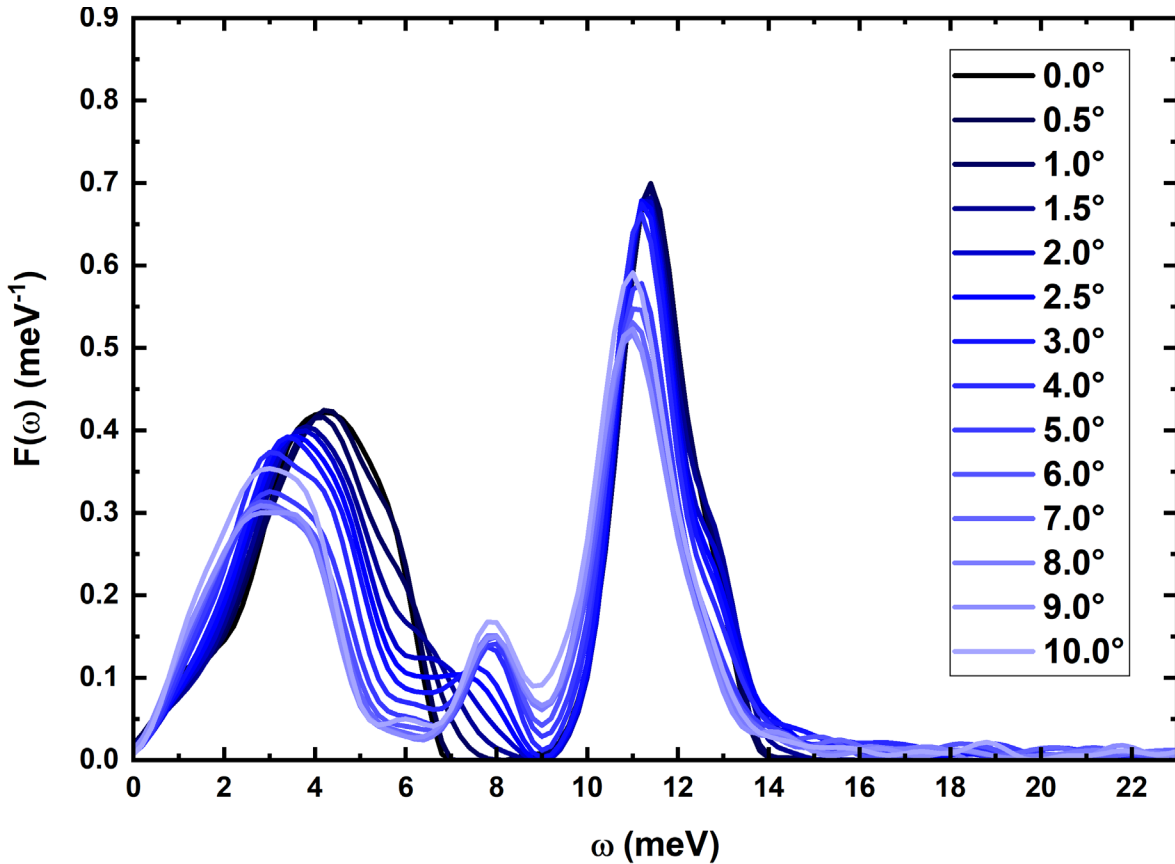


Figure 4. Comparison of the vibrational densities of states ($F(\omega)$), normalized to three modes per atom.

The vibrational density of states ($F(\omega)$) is composed of two primary bands, the acoustic band is located from 0 to about 7 meV (56 cm^{-1} , 1.6 THz) while the optical band is located from around 9 meV (72 cm^{-1} , 3.6 THz) to around 15 meV (120 cm^{-1} , 3.6 THz) for the twist of 0.0° . This is consistent with both experimental and theoretical results for the crystalline structure [33,36] as well as bismuthene (Bismuth (111) Bilayers) [37,51–54].

The forbidden band-gap from around 7 meV to around 9 meV decreases as the bismuthene bilayers are twisted with respect to each other and it completely disappears at the 4.0° rotation, although a minimum at 9 meV is still present for all the studied rotations. The presence of a bimodality in the $F(\omega)$ seems to be a universal characteristic of all 2D materials [55], and this may be due to the existence of layers as demonstrated by our group for 3D materials that have layered structures.

Also, at 2.0° of rotation isolated phonon modes begin to appear above 16 meV, the isolated modes increase in frequency and intensity up to 42 meV for the 10° rotation, although these contributions are small in quantity (less than 0.5% of the modes for the 2.5° sample, and less than 1.8% of the modes for the 10° sample). The relatively high energy of these modes has an impact in related quantities like the Debye frequency and temperature as will be seen in the next section. The existence of these high-energy modes was predicted by Chowdhury [56], and these modes seem to be related to border defects in the bismuthene bilayers.

Superconductivity

Although there seems not to be an agreement in the kind of superconductivity responsible for the magic angle in TBG [28,29], there has been a lot of success using conventional superconductivity for bismuth crystalline phases [33,34,36], as well as for bismuthene bilayers [37].

In order to calculate the superconducting transition temperature, the approach developed by Mata-Valladares [33], is used. The superconducting transition temperature for the crystalline bismuth is calculated with the BCS equation:

$$T_c^\alpha = 1.13\theta_D^\alpha \exp\left(-\frac{1}{N(E_F)^\alpha V_0}\right).$$

Analogously, the superconducting transition temperature for the twisted bismuth bilayers is calculated with the BCS equation:

$$T_c^\beta = 1.13\theta_D^\beta \exp\left(-\frac{1}{N(E_F)^\beta V_0}\right),$$

where we have assumed that the electron-phonon coupling potential V_0 is the same for both materials, the crystalline and the bilayered structures. If we know take the ratio T_c^β/T_c^α and solve for T_c^β , the following equation is obtained:

$$T_c^\beta = (T_c^\alpha)^{1/\varepsilon} \delta \{1.13\theta_D^\alpha\}^{(\varepsilon-1)/\varepsilon},$$

where:

$$N(E_F)^\beta = \varepsilon N(E_F)^\alpha \text{ and } \theta_D^\beta = \delta \theta_D^\alpha.$$

$N(E_F)^\beta$ was calculated directly from Figure 3 and can be seen in Figure 5 A), while θ_D^β was calculated using Grimvall approach [41] and Figure 4, and the results are presented in Figure 5 B). The results considering a frequency cutoff of $\omega_{max} = 23$ meV are shown in red dots, while the results for $\omega_{max} = 50$ meV are shown in black squares. These results offer the exact same θ_D^β up to a twisting angle of 3.0° , and start to differ from 4.0° up to 10.0° . This difference is caused by the high energy isolated modes in the $F(\omega)$. Although these modes represent less than 2% of the total modes calculated, the difference in the Debye temperature can be as large as 6 K for the 9.0° rotation.

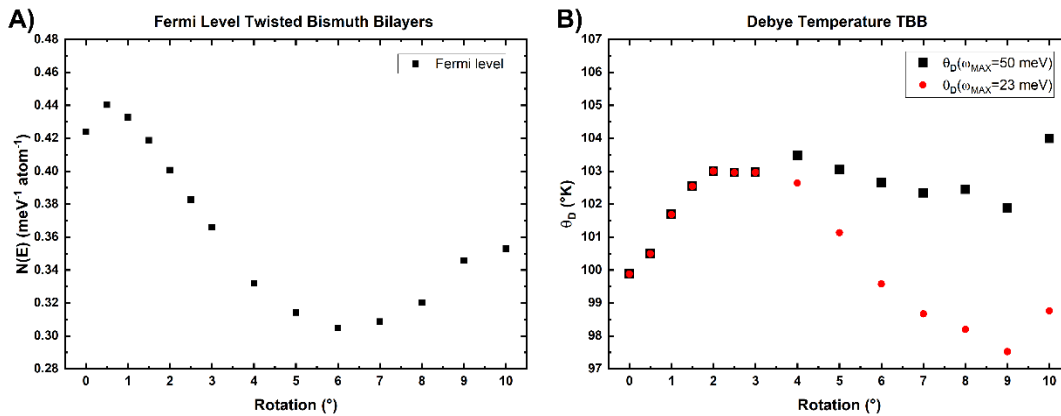


Figure 5. A) Electronic density of states at the Fermi level for the twisted bismuth bilayers and B) Debye temperatures for the twisted bismuth bilayers for two different frequency cut-offs.

Then, using the experimental results for crystalline bismuth: $N(E_F)^\alpha = 0.15 \text{ atom}^{-1}$ and $\theta_D^\alpha = 134.2 \text{ K}$ we calculated the superconducting transition temperatures. The results can be seen in Table 1, and the corresponding Figure 6.

Table 1. Values for the electronic densities of states at Fermi level ($N(E_F)$), Debye temperatures θ_D , the parameters for the Mata-Valladares approach and the superconducting transition temperatures (T_c).

Structure	$N(E_F)$ atom s^{-1}	θ_D (23 meV)	θ_D (50 meV)	ϵ	δ (23 meV)	δ (50 meV)	T_c (23 meV)	T_c (50 meV)
Bi-I	0.15	134.2	134.2	-	-	-	0.0015	0.0015
TBB 0.0°	0.42	99.88	99.88	2.94	0.74	0.74	1.58	1.58
TBB 0.5°	0.44	100.50	100.50	2.88	0.75	0.75	1.85	1.85
TBB 1.0°	0.43	101.69	101.69	2.79	0.76	0.76	1.76	1.76
TBB 1.5°	0.42	102.54	102.54	2.67	0.76	0.76	1.57	1.57
TBB 2.0°	0.40	103.00	103.00	2.55	0.77	0.77	1.32	1.32
TBB 2.5°	0.38	102.96	102.96	2.44	0.77	0.77	1.08	1.08
TBB 3.0°	0.37	102.97	102.97	2.21	0.77	0.77	0.88	0.88
TBB 4.0°	0.33	102.64	103.48	2.10	0.76	0.77	0.55	0.55
TBB 5.0°	0.31	101.14	103.04	2.03	0.75	0.77	0.41	0.41
TBB 6.0°	0.30	99.58	102.65	2.06	0.74	0.76	0.34	0.35
TBB 7.0°	0.31	98.67	102.34	2.14	0.74	0.76	0.36	0.37
TBB 8.0°	0.32	98.20	102.45	2.31	0.73	0.77	0.44	0.45
TBB 9.0°	0.35	97.52	101.89	2.35	0.73	0.76	0.64	0.67
TBB 10.0°	0.36	98.76	104.00	2.83	0.74	0.77	0.72	0.76

The difference in the superconducting transition temperatures is less than 2.7% whether we consider the high-energy vibrational modes above 23 meV, or not. It also appears that superconductivity is mostly driven by the electronic density of states.

The largest T_c found was 1.85 K for a rotation of 0.5° between layers, as can be seen in Figure 6. A more detailed study should be conducted around this angle to find a possible higher maximum or corroborate if the maximum T_c is indeed 1.85 K. The minimum T_c was 0.35 K for a rotation of about 6.0°. For angles above 7.0° the T_c begins to increase again, so higher rotation angles above 10° may have a higher T_c . A more extensive study should be conducted to investigate this surmise.

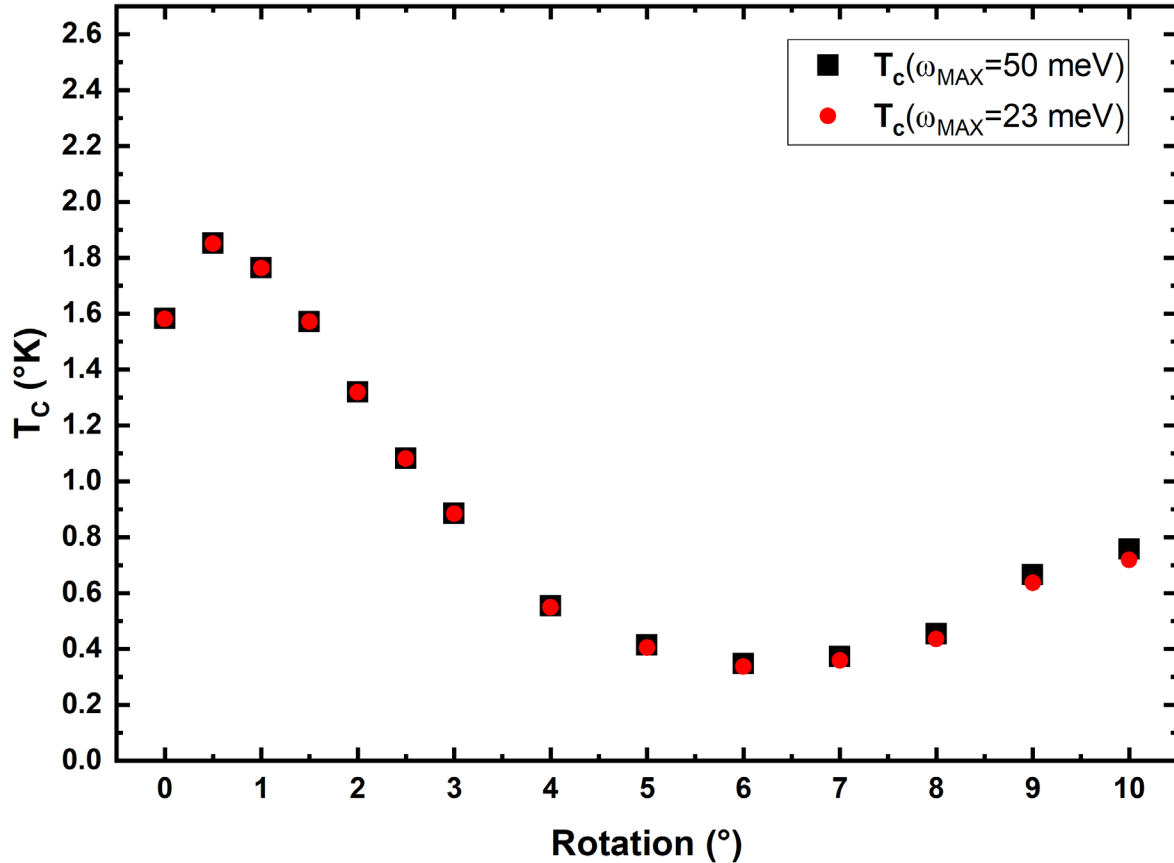


Figure 6. Superconducting critical temperatures for twisted bismuth bilayers.

Conclusions

Twisted bismuth bilayers have shown several interesting properties, such as the presence of Van Hove singularities near the Fermi level, located at the border of the nanolayers, as well as superconductivity for all angles studied, with a maximum of 1.85 K for a rotation of 0.5 ° between layers.

The superconductivity seems to be of the conventional type, and the superconducting transition temperature appears to be electronic driven since calculating the Debye temperature with two different frequency cutoffs have a negligible impact in the superconducting transition temperature.

Acknowledgements

I.R. thanks CONAHCYT, for his postdoctoral fellowship. D.H.-R. acknowledges CONAHCYT for supporting their graduate studies. A.A.V., R.M.V. and A.V. thank DGAPA-UNAM (PAPIIT) for continued financial support to carry out research projects under Grant No. IN116520. María Teresa Vázquez and Oralia Jiménez provided the information requested. Alberto Lopez[†] and Alejandro Pompa assisted with the technical support and maintenance of the computing unit at IIM-UNAM. Simulations were partially carried at the Computing Center of DGTIC-UNAM through project LANCAD-UNAM-DGTIC-131.

Author contributions

I.R. and A.A.V. conceived this research and designed it with the participation of R.M.V., A.V., D.H.-R. All the simulations were done by I.R. All authors discussed and analyzed the results. A.A.V.

wrote the first draft and the other authors enriched the manuscript. All authors gave their consent for the publication of this manuscript.

The authors declare no conflict of interest in this work.

References

- [1] D. Duan, Y. Liu, F. Tian, D. Li, X. Huang, Z. Zhao, H. Yu, B. Liu, W. Tian, and T. Cui, *Pressure-Induced Metallization of Dense (H₂S)₂H₂ with High-T_c Superconductivity*, *Sci Rep* **4**, 6968 (2014).
- [2] A. P. Drozdov, M. I. Erements, I. A. Troyan, V. Ksenofontov, and S. I. Shylin, *Conventional Superconductivity at 203 Kelvin at High Pressures in the Sulfur Hydride System*, *Nature* **525**, 73 (2015).
- [3] H. Liu, I. I. Naumov, R. Hoffmann, N. W. Ashcroft, and R. J. Hemley, *Potential High-T_c Superconducting Lanthanum and Yttrium Hydrides at High Pressure*, *Proc. Natl. Acad. Sci. U.S.A.* **114**, 6990 (2017).
- [4] P. Kong et al., *Superconductivity up to 243 K in the Yttrium-Hydrogen System under High Pressure*, *Nat Commun* **12**, 5075 (2021).
- [5] E. Snider, N. Dasenbrock-Gammon, R. McBride, M. Debessai, H. Vindana, K. Vencatasamy, K. V. Lawler, A. Salamat, and R. P. Dias, *RETRACTED ARTICLE: Room-Temperature Superconductivity in a Carbonaceous Sulfur Hydride*, *Nature* **586**, 373 (2020).
- [6] D. Castelvecchi, *Stunning Room-Temperature-Superconductor Claim Is Retracted*, *Nature* d41586 (2022).
- [7] N. Dasenbrock-Gammon et al., *Evidence of Near-Ambient Superconductivity in a N-Doped Lutetium Hydride*, *Nature* **615**, 244 (2023).
- [8] X. Ming et al., *Absence of Near-Ambient Superconductivity in LuH_{2±x}Ny*, *Nature* **620**, 72 (2023).
- [9] S. Lee, J.-H. Kim, and Y.-W. Kwon, *The First Room-Temperature Ambient-Pressure Superconductor*, arXiv:2307.12008.
- [10] I. Timokhin, C. Chen, Z. Wang, Q. Yang, and A. Mishchenko, *Synthesis and Characterisation of LK-99*, arXiv:2308.03823.
- [11] P. Puphal, M. Y. P. Akbar, M. Hepting, E. Goering, M. Isobe, A. A. Nugroho, and B. Keimer, *Single Crystal Synthesis, Structure, and Magnetism of Pb_{1-x}Cu_x(PO₄)₆O*, arXiv:2308.06256.
- [12] F. B. Quiroga, D. Hinojosa-Romero, A. Valladares, R. M. Valladares, I. Rodríguez, and A. A. Valladares, *The Effect of Negative Pressures on the Superconductivity of Amorphous and Crystalline Bismuth*, *Sci Rep* **12**, 19278 (2022).
- [13] F. Liu, C.-C. Liu, K. Wu, F. Yang, and Y. Yao, *D + i d' Chiral Superconductivity in Bilayer Silicene*, *Phys. Rev. Lett.* **111**, 066804 (2013).
- [14] Y. Zhao, S. Zeng, C. Lian, Z. Dai, S. Meng, and J. Ni, *Multigap Anisotropic Superconductivity in Borophenes*, *Phys. Rev. B* **98**, 134514 (2018).
- [15] D. Pesin and A. H. MacDonald, *Spintronics and Pseudospintronics in Graphene and Topological Insulators*, *Nature Mater* **11**, 409 (2012).
- [16] M. Akhtar, G. Anderson, R. Zhao, A. Alruqi, J. E. Mroczkowska, G. Sumanasekera, and J. B. Jasinski, *Recent Advances in Synthesis, Properties, and Applications of Phosphorene*, *Npj 2D Mater Appl* **1**, 5 (2017).
- [17] L. Xian, A. Pérez Paz, E. Bianco, P. M. Ajayan, and A. Rubio, *Square Selenene and Tellurene: Novel Group VI Elemental 2D Materials with Nontrivial Topological Properties*, *2D Mater.* **4**, 041003 (2017).
- [18] A. Molle and C. Grazianetti, editors, *Xenes: 2D Synthetic Materials beyond Graphene* (Woodhead Publishing, an imprint of Elsevier, Oxford, 2022).

- [19] Ph. Hofmann, *The Surfaces of Bismuth: Structural and Electronic Properties*, Progress in Surface Science **81**, 191 (2006).
- [20] S. Zhang, M. Xie, F. Li, Z. Yan, Y. Li, E. Kan, W. Liu, Z. Chen, and H. Zeng, *Semiconducting Group 15 Monolayers: A Broad Range of Band Gaps and High Carrier Mobilities*, Angew. Chem. **128**, 1698 (2016).
- [21] T. Nagao, J. Sadowski, M. Saito, S. Yaginuma, Y. Fujikawa, T. Kogure, T. Ohno, Y. Hasegawa, S. Hasegawa, and T. Sakurai, *Nanofilm Allotrope and Phase Transformation of Ultrathin Bi Film on Si(111)-7×7*, Phys. Rev. Lett. **93**, 105501 (2004).
- [22] S. Hatta, Y. Ohtsubo, S. Miyamoto, H. Okuyama, and T. Aruga, *Epitaxial Growth of Bi Thin Films on Ge(111)*, Applied Surface Science **256**, 1252 (2009).
- [23] C. Cheng and K. Kunc, *Structure and Stability of Bi Layers on Si(111) and Ge(111) Surfaces*, Phys. Rev. B **56**, 10283 (1997).
- [24] J. E. Moore, *The Birth of Topological Insulators*, Nature **464**, 194 (2010).
- [25] F. Reis, G. Li, L. Dudy, M. Bauernfeind, S. Glass, W. Hanke, R. Thomale, J. Schäfer, and R. Claessen, *Bismuthene on a SiC Substrate: A Candidate for a High-Temperature Quantum Spin Hall Material*, Science **357**, 287 (2017).
- [26] T. Wang, N. F. Q. Yuan, and L. Fu, *Moiré Surface States and Enhanced Superconductivity in Topological Insulators*, Phys. Rev. X **11**, 021024 (2021).
- [27] A. Pezo, B. Focassio, G. R. Schleder, M. Costa, C. Lewenkopf, and A. Fazzio, *Disorder Effects of Vacancies on the Electronic Transport Properties of Realistic Topological Insulator Nanoribbons: The Case of Bismuthene*, Phys. Rev. Materials **5**, 014204 (2021).
- [28] Y. Cao, V. Fatemi, S. Fang, K. Watanabe, T. Taniguchi, E. Kaxiras, and P. Jarillo-Herrero, *Unconventional Superconductivity in Magic-Angle Graphene Superlattices*, Nature **556**, 43 (2018).
- [29] Y. Cao et al., *Correlated Insulator Behaviour at Half-Filling in Magic-Angle Graphene Superlattices*, Nature **556**, 80 (2018).
- [30] J. M. Reynolds and C. T. Lane, *Superconducting Bismuth Alloys*, Phys. Rev. **79**, 405 (1950).
- [31] J. S. Shier and D. M. Ginsberg, *Superconducting Transitions of Amorphous Bismuth Alloys*, Phys. Rev. **147**, 384 (1966).
- [32] S. Fujime, *Electron Diffraction at Low Temperature II. Radial Distribution Analysis of Metastable Structure of Metal Films Prepared by Low Temperature Condensation*, Jpn. J. Appl. Phys. **5**, 764 (1966).
- [33] Z. Mata-Pinzón, A. A. Valladares, R. M. Valladares, and A. Valladares, *Superconductivity in Bismuth. A New Look at an Old Problem*, PLoS ONE **11**, e0147645 (2016).
- [34] O. Prakash, A. Kumar, A. Thamizhavel, and S. Ramakrishnan, *Evidence for Bulk Superconductivity in Pure Bismuth Single Crystals at Ambient Pressure*, Science **355**, 52 (2017).
- [35] A. A. Valladares, I. Rodríguez, D. Hinojosa-Romero, A. Valladares, and R. M. Valladares, *Possible Superconductivity in the Bismuth IV Solid Phase under Pressure*, Sci Rep **8**, 5946 (2018).
- [36] I. Rodríguez, D. Hinojosa-Romero, A. Valladares, R. M. Valladares, and A. A. Valladares, *A Facile Approach to Calculating Superconducting Transition Temperatures in the Bismuth Solid Phases*, Sci Rep **9**, 5256 (2019).
- [37] D. Hinojosa-Romero, I. Rodríguez, A. Valladares, R. M. Valladares, and A. A. Valladares, *Possible Superconductivity in Bismuth (111) Bilayers. Their Electronic and Vibrational Properties from First Principles*, MRS Adv. **3**, 313 (2018).
- [38] B. Delley, *Hardness Conserving Semilocal Pseudopotentials*, Phys. Rev. B **66**, 155125 (2002).
- [39] Dassault Systèmes BIOVIA, *Materials Studio 2016: DMol3* (Dassault Systèmes BIOVIA, 2016).
- [40] S. H. Vosko, L. Wilk, and M. Nusair, *Accurate Spin-Dependent Electron Liquid Correlation Energies for Local Spin Density Calculations: A Critical Analysis*, Can. J. Phys. **58**, 1200 (1980).
- [41] G. Grimvall, *Thermophysical Properties of Materials* (Elsevier, 1999), p. 89-92.

- [42] OriginLab Corporation, *OriginPro, Version 2022b*. (Northampton, MA, USA., 2022).
- [43] G. Jezequel, Y. Petroff, R. Pinchaux, and F. Yndurain, *Electronic Structure of the Bi(111) Surface*, Phys. Rev. B **33**, 4352 (1986).
- [44] G. Jezequel, J. Thomas, and I. Pollini, *Experimental Band Structure of Semimetal Bismuth*, Phys. Rev. B **56**, 6620 (1997).
- [45] Y.-W. Liu, J.-B. Qiao, C. Yan, Y. Zhang, S.-Y. Li, and L. He, *Magnetism near Half-Filling of a Van Hove Singularity in Twisted Graphene Bilayer*, Phys. Rev. B **99**, 201408 (2019).
- [46] R. Pons, A. Mielke, and T. Stauber, *Flat-Band Ferromagnetism in Twisted Bilayer Graphene*, Phys. Rev. B **102**, 235101 (2020).
- [47] K. Dong, T. Zhang, J. Li, Q. Wang, F. Yang, Y. Rho, D. Wang, C. P. Grigoropoulos, J. Wu, and J. Yao, *Flat Bands in Magic-Angle Bilayer Photonic Crystals at Small Twists*, Phys. Rev. Lett. **126**, 223601 (2021).
- [48] Y. Kadioglu, S. B. Kilic, S. Demirci, O. Ü. Aktürk, E. Aktürk, and S. Ciraci, *Modification of Electronic Structure, Magnetic Structure, and Topological Phase of Bismuthene by Point Defects*, Phys. Rev. B **96**, 245424 (2017).
- [49] S.-C. Chen, J.-Y. Wu, and M.-F. Lin, *Feature-Rich Magneto-Electronic Properties of Bismuthene*, New J. Phys. **20**, 062001 (2018).
- [50] C. König, J. C. Greer, and S. Fahy, *Electronic Properties of Bismuth Nanostructures*, Phys. Rev. B **104**, 045432 (2021).
- [51] E. Aktürk, O. Ü. Aktürk, and S. Ciraci, *Single and Bilayer Bismuthene: Stability at High Temperature and Mechanical and Electronic Properties*, Phys. Rev. B **94**, 014115 (2016).
- [52] M. Pumera and Z. Sofer, *2D Monoelemental Arsenene, Antimonene, and Bismuthene: Beyond Black Phosphorus*, Adv. Mater. **29**, 1605299 (2017).
- [53] T. Chai, X. Li, T. Feng, P. Guo, Y. Song, Y. Chen, and H. Zhang, *Few-Layer Bismuthene for Ultrashort Pulse Generation in a Dissipative System Based on an Evanescent Field*, Nanoscale **10**, 17617 (2018).
- [54] H. Pei, Y. Wei, X. Guo, and B. Wang, *Raman Scattering Spectra of Bismuthene: A First-Principles Prediction*, Optik **180**, 967 (2019).
- [55] J. C. Noyola-Pineda and A. Valladares, *The Effect of Porosity on the Vibrational and Low Temperature Equilibrium Thermodynamic Properties of Amorphous Silicon via Computer Simulation*, J. Non-Cryst. Solids **455**, 42 (2017).
- [56] E. H. Chowdhury, Md. H. Rahman, P. Bose, R. Jayan, and M. M. Islam, *Atomic-Scale Analysis of the Physical Strength and Phonon Transport Mechanisms of Monolayer β -Bismuthene*, Phys. Chem. Chem. Phys. **22**, 28238 (2020).